PHYSICAL REVIEW A **86**, 040701(R) (2012)

Feshbach resonances in cesium at ultralow static magnetic fields

D. J. Papoular,[1,2] S. Bize,[3] A. Clairon,[3] H. Marion,[3] S. J. J. M. F. Kokkelmans,[4] and G. V. Shlyapnikov[2,5]
[1]*INO-CNR BEC Center and Dipartimento di Fisica, Università di Trento, 38123 Povo, Italy*
[2]*Laboratoire de Physique Théorique et Modèles Statistiques, CNRS, Université Paris-Sud, F-91405, Orsay, France*
[3]*LNE-SYRTE, Observatoire de Paris, CNRS, UPMC, F-75014 Paris, France*
[4]*Eindhoven University of Technology, Post Office Box 513, 5600 MB Eindhoven, The Netherlands*
[5]*Van der Waals–Zeeman Institute, University of Amsterdam, Science Park 904, 1098 XH Amsterdam, The Netherlands*
(Received 11 May 2012; published 24 October 2012)

We have observed Feshbach resonances for ^{133}Cs atoms in two different hyperfine states at static magnetic fields of a few milligauss. These resonances are unusual for two main reasons. First, they are the lowest static-field resonances investigated up to now, and we explain their multipeak structure in these ultralow fields. Second, they are robust with respect to temperature effects. We have measured them using an atomic fountain clock and reproduced them using coupled-channels calculations, which are in excellent agreement with our measurements. We show that these are *s*-wave resonances due to a very weakly bound state of the triplet molecular Hamiltonian. We also describe a model explaining their asymmetric shape in the regime where the kinetic energy dominates over the coupling strength.

DOI: 10.1103/PhysRevA.86.040701 PACS number(s): 34.50.Cx, 67.85.−d, 06.30.Ft, 37.10.Vz

The achievement of Bose-Einstein condensation [1] has stimulated remarkable developments in atomic physics. Ultracold atoms have found applications in metrology [2] and high-precision measurements of physical constants [3]; they can be cooled down to quantum degeneracy and used to simulate condensed-matter systems [4,5]. A fundamental feature of ultracold atomic gases, underlying most of their present applications, is that the interparticle interactions can be tailored at will, using scattering resonances that occur in low-energy collisions between two atoms [6]. These Feshbach resonances are usually obtained using an external static magnetic field [7]. Their accurate characterization is intimately linked to a detailed knowledge of the interatomic interaction [8] and involves coupled-channels calculations [9].

We report on the measurement of multiple Feshbach resonances in ^{133}Cs using an atomic fountain clock and present their theoretical characterization using the coupled-channels method. These resonances are unusual for two main reasons. First, they occur at very low magnetic fields of the order of a few milligauss, which makes them the lowest-static-field resonances investigated up to now. In these ultralow fields, the quasidegeneracy of spin-triplet collisional channels plays a key role and conveys a multipeak structure to the resonances. Second, they are robust with respect to temperature effects. We have measured them in a regime where the kinetic energy dominates over the resonance width, and they appear in the magnetic field dependence of the clock shift as asymmetric features close to the zero-temperature resonant field.

The physics we describe in this Rapid Communication is closely linked to the very large and positive value of the triplet scattering length for Cs [8], which exceeds the range of the triplet potential and signals that the highest-energy bound state in this potential is very close to the continuum. This is a specific property of cesium, and a similar situation is encountered in some other systems (e.g., metastable triplet helium [10] and ^{87}Rb ^{133}Cs mixtures [11]). The extreme accuracy of frequency measurements in modern atomic clocks provides the means to reveal effects of atomic collisions in a regime of very weak interactions. The low-field resonances which we describe in this Rapid Communication could be further characterized using density-independent interferometry [12]. This would allow for a probe of the constancy of the proton-to-electron mass ratio and the fine structure constant by exploiting the enhanced sensitivity to their values near a Feshbach resonance [13,14]. Furthermore, these resonances involve atoms in two different spin states and thus pave the way for the study of quantum magnetism in ultracold cesium gases containing two different hyperfine states.

Experimental setup. The experiment is done in a fountain geometry, which has already been described extensively (see, e.g., Ref. [2]) and which is sketched in Fig. 1. A cloud of ^{133}Cs atoms, launched and laser cooled to $\sim$1 μK, is prepared to contain atoms in two different states: $|f = 3, m_f = 0\rangle$ and $|f = 3, m_f \neq 0\rangle$. It undergoes a ballistic flight inside the fountain. The interaction between the atoms causes the apparent frequency of the $|f = 3, m_f = 0\rangle \rightarrow |f = 4, m_f = 0\rangle$ "clock" transition to differ from the hyperfine transition frequency of a single atom. This frequency shift, known as the collisional "clock shift," is measured by Ramsey interferometry [15]: The atom cloud goes through the microwave cavity twice, once at the beginning and once at the end of the flight [16], whose duration is called the interrogation time. The transition probability to the $f = 4$ hyperfine state, plotted as a function of the microwave frequency, shows interference fringes. The fringe width is inversely proportional to the interrogation time and is $<$1 Hz, making Ramsey interferometry an ideal tool for frequency metrology.

Clock shift measurements of Feshbach resonances. The clock shift depends on elementary collisional properties, which are affected by the presence of a magnetic field. We exploit this dependence to observe Feshbach resonances by measuring the clock shift. This observable is very sensitive to the atomic spatial and velocity distributions, first because of the evolution of the atomic cloud during the interrogation (see, e.g., Ref. [17]), and second because the measured shifts are strongly sensitive to the collision energy. In order to minimize the

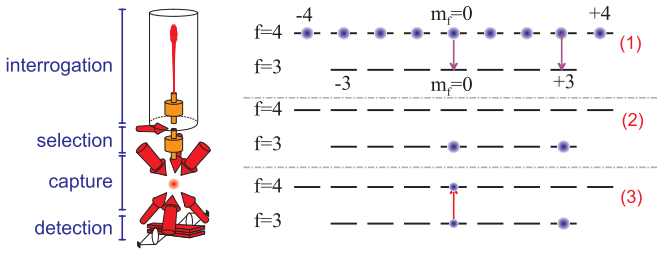

FIG. 1. (Color online) Left: schematics of the atomic fountain. Right: hyperfine levels used in the experiment. Populations after launch and transitions excited for the state preparation (1). A horizontal laser beam then pushes away $f = 4$ atoms. Populations at the start (2) and during (3) the interrogation.

impact of the atomic distributions, we determine collision shift ratios by performing interleaved frequency measurements with three configurations, leading to three measured frequencies: $\nu_0^{(1)}$, $\nu_0^{(1/2)}$, and $\nu_{0;m_f}^{(1)}$. First, the $|3,m_f = 0\rangle$ state is selected with the maximum possible atom number N_0. Second, the $|3,m_f = 0\rangle$ state is selected with the atom number $N_0/2$. Third, N_0 atoms in $|3,m_f = 0\rangle$ are selected together with N_{m_f} atoms in another chosen $|3,m_f\rangle$ state, as illustrated in Fig. 1 for $m_f = 3$. The expanding atomic cloud is truncated during the Ramsey cavity traversals, so that the detected atoms are only a fraction ($\sim$20%) of the initially selected atoms, and N_0, $N_0/2$, and N_{m_f} refer to the detected atom numbers. A crucial feature of our experiment is to perform the microwave excitation for state selection with the (interrupted-) adiabatic passage method described in Ref. [18] in order to ensure quasi-identical space and velocity distributions for all states and all configurations. We can prepare the third configuration with any of the six $m_f = \pm1, \pm2, \pm3$ states. Typically, $N_0 \approx N_{m_f} \sim 5 \times 10^6$. The corresponding effective density during the interrogation is $\sim 2 \times 10^7\,\mathrm{cm}^{-3}$, many orders of magnitudes lower than in typical quantum gas experiments.[1] The mean free path is $\sim$35 m and the mean time between collisions is $\sim$5000 s, that is, 3 orders of magnitude longer than the experimental cycle.

In a given configuration, the frequency shift of the $|3,0\rangle \longrightarrow |4,0\rangle$ transition is given by

$$\delta\nu = n_0\rho_0 K_0(B,\mathcal{D}_{r,v}) + n_{m_f}\rho_{m_f} K_{m_f}(B,\mathcal{D}_{r,v}), \tag{1}$$

where n_0 and n_{m_f} are the detected atom numbers, ρ_0 and ρ_{m_f} are the effective densities per detected atom, and K_0 and K_{m_f} are the collision shifts scaled to the effective densities. These functions depend on the space and velocity distributions $\mathcal{D}_{r,v}$, and more generally on the fountain geometry. They include collisional properties and thus also depend on the magnetic field B, which is known via the spectroscopy of the first-order-sensitive $|3,m_f = 1\rangle \rightarrow |4,m_f = 1\rangle$ transition. It is stable to $\sim$40 nG and homogeneous to better than 10^{-2}.

[1]The dominant processes that will smear out our resonances at large densities are two-body inelastic collisions. They are efficient at densities of $>10^{13}\,\mathrm{cm}^{-3}$. However, for densities $\sim 10^{13}\,\mathrm{cm}^{-3}$ (typical in experiments with ultracold gases), mixtures containing both $f = 4$ and $f = 3$ atoms have an inverse lifetime which we estimate to be $\sim 100\,\mathrm{s}^{-1}$ (i.e., 0.1 mG in magnetic field units), which makes the resonances insensitive to inelastic decay.

It keeps the same downward orientation over the entire height of the fountain to avoid spin-flip losses and to ensure a good control of the quantization axis. Under these conditions, selecting a $-m_f$ state for a measurement is equivalent to probing the $+m_f$ state with the field $-B$. Starting from the measured frequency shifts and the detected atom numbers, we compute the shift per detected $m_f = 0$ atom, $A_{0;0}$, and the additional shift $A_{m_f;0}$ due to the $m_f \neq 0$ population, per detected $m_f \neq 0$ atom:

$$\begin{aligned} A_{0;0} &= \frac{\nu_0^{(1)} - \nu_0^{(1/2)}}{N_0 - N_0/2} = \rho_0 K_0(B,\mathcal{D}_{r,v}), \\ A_{m_f;0} &= \frac{\nu_{0;m_f}^{(1)} - \nu_0^{(1)}}{N_{m_f}} = \rho_{m_f} K_{m_f}(B,\mathcal{D}_{r,v}). \end{aligned} \tag{2}$$

The (B-independent) densities ρ_0 and ρ_{m_f} are almost equal. Hence, the ratio $R_{m_f,0}(B) = A_{m_f;0}/A_{0;0} \simeq K_{m_f}/K_0$ does not depend on the detected atom numbers and is as close to intrinsic collisional properties as possible in our experiment. We have determined $A_{0;0}$, $A_{m_f;0}$, and $R_{m_f;0}$, for B ranging from 0 to 100 mG, for the three possible additional states $m_f = 1$, 2, or 3. Our measurements of $R_{m_f;0}(B)$ are shown in Fig. 2, and they exhibit a dramatic dependence of $R_{m_f;0}$ on B for all three states. Instead, we measure no change of the clock collision shift $A_{0;0}(B)$, at a level limited by its dependence on ρ_0, and thus on the atomic distributions $\mathcal{D}_{r,v}$. Within these limits, K_0 remains constant over the entire range of our experiments. It is equal to the large negative clock shift which affects Cs fountain clocks [19–21]. Hence, the observed behavior of $R_{m_f;0}(B)$ relates to $K_{m_f}(B,\mathcal{D}_{r,v})$, which we attribute to Feshbach resonances either in the $|3,0;3,m_f\rangle$ or the $|4,0;3,m_f\rangle$ channel.

The precise control of the magnetic field and the high signal-to-noise ratio of the data allow for a stringent comparison to two theoretical approaches: (i) a coupled-channels calculation of the scattering length characterizing interactions at zero temperature as a function of B, and (ii) a finite-temperature model of the clock collision shift in the fountain geometry, which explains the asymmetric shape of the observed resonances.

Calculation of the scattering length. We describe the system in the center-of-mass frame of the atom pair. Neglecting the spin-spin interaction, which yields no significant contribution to our observables, the interaction is spatially isotropic. We limit our analysis to s-wave interactions governed by the following Hamiltonian [9]:

$$H = \frac{p^2}{2\mu} + V_{\mathrm{el}}(r) + V_{\mathrm{hf}} + V_{\mathrm{Z}}, \tag{3}$$

where r is the interatomic distance, p is its conjugate momentum, and $\mu = m/2$ is the reduced mass of the atom pair. The central part of the interaction is given by $V_{\mathrm{el}}(r) = V_S(r)P_S + V_T(r)P_T$, where P_S and P_T are the projectors onto the electronic singlet and triplet subspaces. The term $V_{\mathrm{hf}} = a_{\mathrm{hf}}(\boldsymbol{s}_1 \cdot \boldsymbol{i}_1 + \boldsymbol{s}_2 \cdot \boldsymbol{i}_2)/\hbar^2$ is the hyperfine interaction, where $\boldsymbol{s}_j$ and $\boldsymbol{i}_j$ are the spin operators of the electron and the nucleus of atom j. The operator $V_{\mathrm{Z}} = 2\mu_B B\, S_z$ is the Zeeman term, with μ_B being the Bohr magneton and $S_z = s_{1z} + s_{2z}$ being the total electronic spin projection along the quantization axis $\boldsymbol{e}_z$.

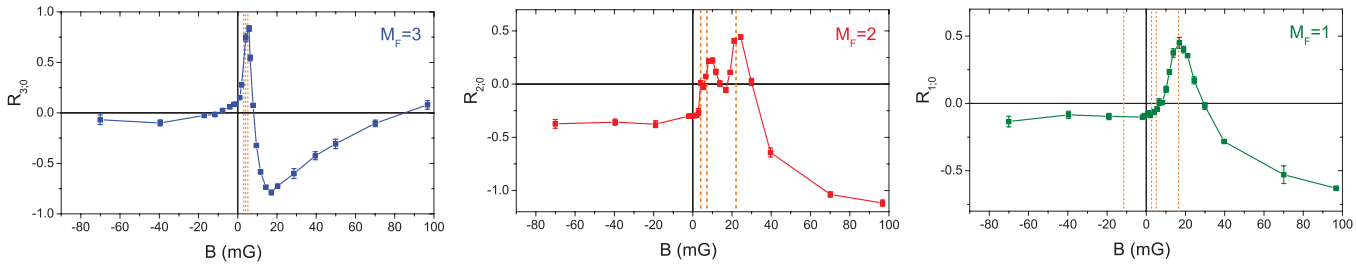

FIG. 2. (Color online) Measured collision frequency shift ratio $R_{m_f;0}(B)$ from the experiment, exhibiting Feshbach resonances at ultralow static magnetic fields. Left: $M_F = 3$; middle: $M_F = 2$; right: $M_F = 1$. The vertical lines show the theoretical resonant field values. Experiment (effective temperature ~900 nK) and theory ($E = 0$, Fig. 3) are completely independent (see text).

We calculate the B-dependent scattering length associated with the zero-energy scattering state corresponding to the levels populated in the experiment. The Hamiltonian H conserves the projection M_F of the total two-atom spin $\boldsymbol{F} = \boldsymbol{f}_1 + \boldsymbol{f}_2$, where $\boldsymbol{f}_j = \boldsymbol{s}_j + \boldsymbol{i}_j$ is the total spin of atom j. Therefore, this scattering state has a definite value of the total spin projection M_F, on which the scattering length $a_{M_F}(B)$ depends. For large interatomic separations, the atoms are in the Zeeman-dressed state related to the (Bose-symmetrized) two-atom state $|f_1 = 4, m_1 = 0; f_2 = 3, m_2 = M_F\rangle$, where f_j and m_j define the magnitude and projection of the total spin $\boldsymbol{f}_j$. The measurements shown in Fig. 2 relate to $M_F = 3$, 2, and 1. The corresponding scattering state $|\Psi_{M_F,B}\rangle$ has 10, 13, and 14 components, respectively. We evaluate it numerically using the coupled-channels approach [9], our implementation of which is described in Ref. [22]. The accumulated-phase-boundary condition [9] is applied at $r_0 = 20\,a_0$, and the asymptotic behavior of the scattering state is enforced at $r_{\max} = 1000\,a_0$. The values of the accumulated-phase parameters, the hyperfine interaction constant $a_{\rm hf}$, and the electronic potentials V_S and V_T are the same as those used in Ref. [23].

Our results for the s-wave scattering length $a_{M_F}(B)$ are shown in Fig. 3, for $M_F = 3$, 2, and 1. The occurrence of inelastic processes (such as the decay towards the lower-energy states having $f_1 = f_2 = 3$) causes a to have a nonvanishing imaginary part [24] and the resonances appear as smooth dispersive features (rather than as the divergences of the lossless case). The calculated positions of the broadest resonances compare favorably to those determined from the clock-shift measurements (Fig. 2). The predicted multiple-peak structure is clearly visible in the experimental data for $M_F = 2$.

Our numerical analysis includes only s–wave interactions, and the fact that it recovers the measured resonance positions proves that these are s–wave resonances. The triplet potential V_T supports a very weakly bound state, with the binding energy $|E_T| = \hbar^2/(2\mu a_T^2) \approx h\,5\,\text{kHz} = \mu_B\,4\,\text{mG}$, where $a_T = 2400\,a_0$ is the scattering length associated with V_T [8]. For a given value of M_F, the two-atom internal states $|f_1 = 4, f_2 = 3, F, M_F\rangle$ are electronic triplets for all allowed odd values of F. For $B = 0$, each of these triplet channels supports the weakly bound triplet state, yielding N_M^T degenerate bound states (energy $-|E_T|$), where N_M^T is the number of triplet channels with the quantum numbers $(f_1 = 4, f_2 = 3, M_F)$. For nonzero, albeit small, magnetic fields, the coupling due to V_Z lifts this degeneracy, and these N_M^T states cross the threshold for different values of B, causing multiple resonances. For $M_F = 3$ or 2, there are $N_M^T = 3$ triplet channels ($F = 7, 5,$ or 3), which correspond to the three predicted resonances in these two cases. For $M_F = 1$, there are $N_1^T = 4$ triplet states ($F = 7, 5, 3, 1$), but our coupled-channels results only show three resonances for $B > 0$. An additional feature is visible for $B \approx -10$ mG, which could be a signature of the expected fourth resonance. Its occurrence for negative B and a qualitative difference of the shape from those of the other predicted resonances would be due to the finite lifetime of a resonant triplet state which has become quasibound [25]. This multiple-resonance physics only occurs for small B: indeed, for values of B larger than a few $|E_T|/\mu_B$, the Zeeman term V_Z causes the bare weakly bound triplet states to dissolve into the continuum.

Feshbach resonances in a fountain geometry. To clarify the impact of finite temperatures, the atomic distribution $\mathcal{D}_{r,v}$,

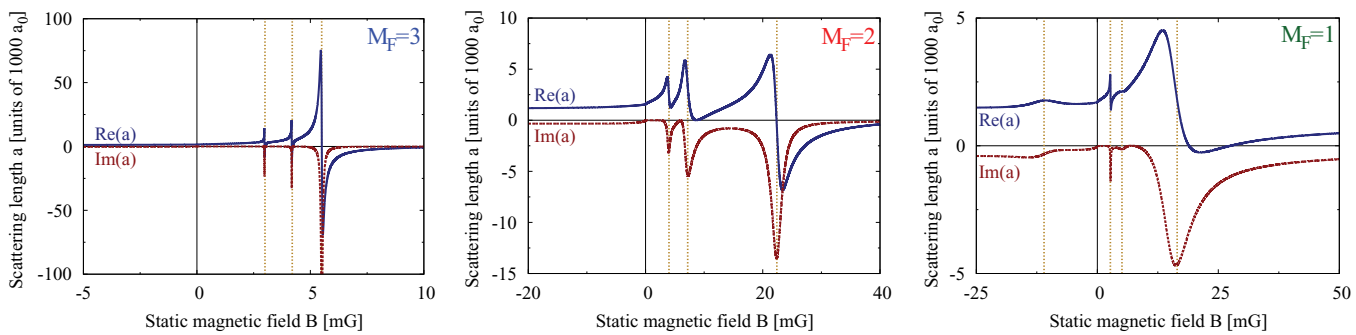

FIG. 3. (Color online) Numerical results for the scattering length $a_{M_F}(B)$, calculated using the coupled-channels method ($E = 0$). Left: $M_F = 3$; middle: $M_F = 2$; right: $M_F = 1$.

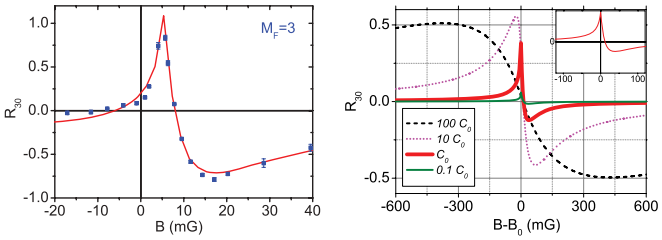

FIG. 4. (Color online) Left: fit of our model [Eqs. (4) and (5)] to the $M_F = 3$ measurements. Right: clock shift as a function of B for various coupling strengths C_e. The value $C_e = C_0 = 4\,E_{\rm rec}/k_{\rm rec}$ (thick red [gray]) is close to the experimental situation; results for $C_e = 100\,C_0$ (dashed black), $10\,C_0$ (dotted magenta [light gray]), and $0.1\,C_0$ (solid green [dark gray]) are also shown. Inset: closeup of the red [gray] curve for small B.

and the fountain geometry, we evaluate the clock shift using a simple model for the S-matrix elements $S_{\alpha\gamma}(k)$ and $S_{\beta\gamma}(k)$ describing the interaction between the clock states, $\alpha = |3,0\rangle$ and $\beta = |4,0\rangle$, and the state $\gamma = |3,m_f\rangle$. The elementary clock shift due to γ is

$$\frac{\delta\omega_{\beta\alpha}}{2\pi} = \frac{\hbar\rho_\gamma}{mk}\,\mathrm{Im}\{S_{\alpha\gamma}(k)S^\dagger_{\beta\gamma}(k) - 1\}, \tag{4}$$

with ρ_γ being the local density of atoms in the state γ and $k = p/\hbar$ being the wave vector for the relative motion of the two colliding atoms. We take $S_{\alpha\gamma}(k) = 1$ and assume a single-resonance behavior for $S_{\beta\gamma}(k)$:

$$S_{\beta\gamma}(k) = 1 - \frac{i\Gamma_e}{E - \Delta\mu(B - B_0) + i\Gamma_e/2}\,, \tag{5}$$

where $E = \hbar^2k^2/2\mu$ is the relative kinetic energy of the colliding pair, $\Delta\mu$ is a relative magnetic moment, B_0 is the zero-energy resonant field, and $\Gamma_e = kC_e$ is the elastic width of the resonance [26], the coupling strength C_e being constant. We have omitted the inelastic contribution to the width, $i\Gamma_i/2$, in the denominator of Eq. (5), as our coupled-channels results imply that $\Gamma_i/C_e \ll k$.

The total clock shift is obtained by averaging Eq. (4) over the measured $\mathcal{D}_{r,v}$. We calculate it using a Monte Carlo simulation accounting for the collisional energy distribution (corresponding to the effective temperature ~900 nK), the decrease of the atomic density with time, and the truncation of the atomic cloud in the microwave resonator. A fit of our model [Eqs. (4) and (5)] to the measurements for $M_F = 3$ [Fig. 4 (left)] yields $B_0 = 5 \pm 1$ mG, $\Delta\mu = 1.5\mu_B$, and $C_e = C_0 = 4E_{\rm rec}/k_{\rm rec}$, where $\hbar k_{\rm rec} = h/\lambda$ and $E_{\rm rec} = \hbar^2k^2_{\rm rec}/2m$ are the recoil momentum and energy, and $\lambda = 852$ nm is the laser cooling wavelength. The fit captures the main features of the data, in particular its asymmetry. Were the resonance to occur in the $\alpha\gamma$ channel, the sign of the clock shift would be reversed. Therefore, this analysis, independent of our coupled-channels results, confirms that the resonance occurs in the $\beta\gamma$ channel.

Finally, we consider the role of the coupling strength compared to the kinetic energy. Figure 4 (right) shows the total clock shift as a function of B for various coupling strengths C_e, keeping B_0 and $\Delta\mu$ fixed to their experimental values. The black curve is for $C_e = 400E_{\rm rec}/k_{\rm rec}$. In this strong-coupling regime, the resonance has a symmetrical dispersive-like shape. At any given field, all atoms within the distribution $\mathcal{D}_{r,v}$ contribute to it, and the collision shift reaches the unitarity limit. The green curve ($C_e = 0.4E_{\rm rec}/k_{\rm rec}$) illustrates the weak-coupling regime, in which the kinetic energy exceeds the elastic width. In this regime, the resonance curve is strongly asymmetric. For $B < B_0$, the resonant channel is closed and the behavior is similar to the far-detuned strong-coupling case. For $B > B_0$, the resonant channel is open. At a given field, only a fraction of the distribution $\mathcal{D}_{r,v}$ contributes significantly to the frequency shift because of the narrow elastic width. Consequently, the total clock shift is smaller than the unitarity limit value. The experimental value $C_e = C_0 = 4E_{\rm rec}/k_{\rm rec}$ (thick red [gray]) is near the weak-coupling regime. The resonant behavior of the clock shift is apparent, and it occurs at B_0, where this model predicts a singularity even at finite temperature.

The presence of the weakly bound triplet state, responsible for our ultralow-field resonances, is a lucky accident in three dimensions (3D). However, weakly bound two-particle states can emerge generically in strongly confined geometries, for example in the quasi-two-dimensional (quasi-2D) case at a negative and fairly small 3D scattering length [27]. The use of this type of states can make ultralow-field resonances a generic feature in quantum gases.

Acknowledgments. We acknowledge many fruitful discussions with J. Dalibard, P. Rosenbusch, C. Salomon, and J. T. M. Walraven.

[1] M. H. Anderson *et al.*, Science **269**, 198 (1995); C. C. Bradley, C. A. Sackett, J. J. Tollett, and R. G. Hulet, Phys. Rev. Lett. **75**, 1687 (1995); K. B. Davis *et al.*, *ibid.* **75**, 3969 (1995).

[2] J. Guéna *et al.*, IEEE Trans. Ultrason. Ferroelectr. Freq. Control **59**, 391 (2012).

[3] F. Biraben, Eur. Phys. J.-Special Topics **172**, 109 (2009).

[4] I. Bloch, J. Dalibard, and W. Zwerger, Rev. Mod. Phys. **80**, 885 (2008).

[5] S. Giorgini, L. P. Pitaevskii, and S. Stringari, Rev. Mod. Phys. **80**, 1215 (2008).

[6] C. Chin, R. Grimm, P. Julienne, and E. Tiesinga, Rev. Mod. Phys. **82**, 1225 (2010).

[7] S. Inouye *et al.*, Nature (London) **392**, 151 (1998).

[8] C. Chin *et al.*, Phys. Rev. A **70**, 032701 (2004).

[9] B. J. Verhaar, E. G. M. van Kempen, and S. J. J. M. F. Kokkelmans, Phys. Rev. A **79**, 032711 (2009).

[10] W. Vassen *et al.*, Rev. Mod. Phys. **84**, 175 (2012).

[11] T. Takekoshi *et al.*, Phys. Rev. A **85**, 032506 (2012).

[12] R. A. Hart, X. Xu, R. Legere, and K. Gibble, Nature (London) **446**, 892 (2007).

[13] C. Chin and V. V. Flambaum, Phys. Rev. Lett. **96**, 230801 (2006).

[14] A. Borschevsky, K. Beloy, V. V. Flambaum, and P. Schwerdtfeger, Phys. Rev. A **83**, 052706 (2011).

[15] N. R. Ramsey, Phys. Rev. **78**, 695 (1950).

[16] A. Clairon, C. Salomon, S. Guellati, and W. D. Phillips, Europhys. Lett. **16**, 165 (1991).

[17] Y. Sortais *et al.*, Phys. Rev. Lett. **85**, 3117 (2000).
[18] F. P. Dos Santos *et al.*, Phys. Rev. Lett. **89**, 233004 (2002).
[19] K. Gibble and S. Chu, Phys. Rev. Lett. **70**, 1771 (1993).
[20] A. Clairon *et al.*, IEEE Trans. Instrum. Meas. **44**, 128 (1995).
[21] P. J. Leo, P. S. Julienne, F. H. Mies, and C. J. Williams, Phys. Rev. Lett. **86**, 3743 (2001).
[22] D. J. Papoular, *Manipulation of Interactions in Quantum Gases: A Theoretical Approach*, Ph.D. thesis, Université Paris-Sud, 2011 [http://tel.archives-ouvertes.fr/tel-00624682].
[23] D. J. Papoular, G. V. Shlyapnikov, and J. Dalibard, Phys. Rev. A **81**, 041603(R) (2010).
[24] L. D. Landau and I. M. Lifschitz, *Quantum Mechanics: Non-relativistic Theory*, 3rd ed. (Pergamon Press, Oxford, 1991).
[25] B. Marcelis, E. G. M. van Kempen, B. J. Verhaar, and S. J. J. M. F. Kokkelmans, Phys. Rev. A **70**, 012701 (2004).
[26] A. J. Moerdijk, B. J. Verhaar, and A. Axelsson, Phys. Rev. A **51**, 4852 (1995).
[27] D. S. Petrov and G. V. Shlyapnikov, Phys. Rev. A **64**, 012706 (2001).